I-1. PROJECT RESEARCHES

Project 8

PR8 Development on Neutron Imaging Application

Y. Saito

Institute for Integrated Radiation and Nuclear Science, Kyoto University

1. Objectives and Allotted Research Subjects: Neutron imaging provides valuable information which cannot be obtained from an optical or X-ray imaging. The purpose of this project is to develop the imaging method itself and also the experimental environment for expanding the application area of the neutron imaging. The allotted research subjects are as follows:

ARS-1: Measurements of Multiphase Dynamics by Neutron Radiography (Y. Saito et al.)
ARS-2: Void Fraction Measurement of Refrigerant Two-Phase Flows in Cross-Flow Parallel Mini-Channel Evaporator (H. Asano et al.)
ARS-3: Visualization of Transient Change of Refrigerant Distribution in Activated Carbon Particle Layer (H. Asano et al.)
ARS-4: Neutron radiography measurements of the mixing behavior of reactant streams during hydrothermal synthesis (S. Takami et al.)
ARS-5: Quantatively Visualization of a Microchannel Heat Exchanger under Non-uniformly Heated Condition (H. Umekawa et al.)
ARS-6: Frost Deposition Distribution Estimated by X-ray and Neutron Cooperative Imaging (R. Matsumoto et al.)
ARS-7: 3D Imaging of Plant roots (U. Matsushima et al.)
ARS-8: Analysis of vapor pressure in fire spalling of high-strength concrete (M. Kanematsu et al.)
ARS-9: Measurement of coolant inside a flat laminate vapor chamber in the vertical posture with Neutron Radiography (K. Mizuta et al.)
ARS-10: Visualization of Organic Materials for Development of Industrial Applications (M. Kitaguchi et al.)
ARS-11: Visualization of Excimer cluster tracers by using Neutrons (Y. Tsuji et al.)
ARS-12: Development of Neutron Imaging Techniques and Its Application (T. Sakai et al.)
ARS-13: Dynamic Visualization of Hydrogen Accumulation Behavior in Metallic Materials via Neutron Imaging (K. Shimizu et al.)
ARS-14: In-situ Lithium diffusion behavior in NASICON-Type Structured Lithium Ion Conductive Composite by Means of Neutron Radiography (S. Takai et al.)

2. Main results and the contents of this report: To develop neutron imaging, our imaging system was developed so that high-speed imaging could be per-formed at thermal neutron flux of 10^7 n/cm^{2}s. Such improved system was shared with all of the project members and valuable results were obtained as follows:

ARS-1 improved the above-mentioned high-speed imaging system at the B4 port. The spatial and temporal resolution of the system was tested. Then, the present system was applied to investigate the effect of motion blur in the observation of rapidly moving object and to visualize particle motions dropped in a molten glass.
ARS-2 applied to neutron imaging to refrigerant two-phase flows in a cross-flow parallel mini-channel evaporator. HFC-134a and FC3283 were used as the refrigerant. From the measurement results, the effect of rib in the mini-channel was clarified in the two-dimensional void fraction distributions. It indicates that the offset rib is not effective.
ARS-3 applied neutron imaging to measurements of refrigerant distribution in activated carbon, which is strongly related to the performance of adsorption refrigerator. Liquid ethanol was used as the refrigerant. Transient change of the refrigerant in the activated carbon particle layer.
ARS-4 applied neutron imaging to the flow visualization of mixing behavior of reactant streams during hydrothermal synthesis. Water and Aqueous solution of GD(CH3C)3 was fed into T-junction tube using high pressure pumps, simultaneously. Due to the attenuation of neutron in Gd in the aqueous solutions, the mixing behavior was clearly visualized.
ARS-5 applied the neutron imaging to boiling two-phase flow in a microchannel heat exchanger under non-uniformly heated conditions. The effect of heat flux distributions on the heat transfer was estimated.
ARS-6 applied neutron imaging to frosting behavior in cooling heat exchange system. Simultaneous Xray and neutron imaging was performed to clarify the 3D frost deposition at the B4 port.
ARS-8 applied neutron imaging to analysis of vapor pressure in fire spalling of high-strength concrete. Measuring moisture transfer inside concrete quantitatively, how vapor pressure inside concrete affect spalling was considered.
ARS-9 applied neutron imaging to measurements of coolant distribution in a flat laminate vapor chamber. Experiments were performed at the E2 port. Measurement results indicate that the liquid thickness depends mainly on the inner structure of the vapor chamber rather than its outer size and shape.
ARS-13 performed dynamic visualization of hydrogen accumulation behavior in metallic materials. However, the contrast of image was not enough. Probably the absolute value of the hydrostatic stress was relatively low, or the size of the formed hydrostatic stress field was much smaller that the spatial resolution of the detector system.
ARS-14 applied to in-situ Lithium diffusion behavior in NASICON-Type structured Lithium Ion conductive composite. From measurement results, it indicates that the material should be changed.

PR8-1 Measurements of multiphase flow dynamics using neutron radiography

Y. Saito, D. Ito and N. Odaira

Institute for Integrated Radiation and Nuclear Science, Kyoto University

INTRODUCTION: Neutron radiography (NRG) is a powerful tool for multiphase flow visualization. Especially, it is possible to observe the flow at high temperature and pressure conditions using NRG. In this work, our neutron imaging system was improved to observe the dynamic two-phase flows. With the improved system, particle motions in a high temperature molten glass was visualized.

IMPROVEMENT OF HIGH-SPEED NEUTRON IMAGING SYSTEM: A high-speed neutron imaging system for flow visualization has been developed at the B-4 supermirror neutron guide facility [1] of the Institute for Integrated Radiation and Nuclear Science, Kyoto University. Using the system with an optical image intensifier, a frame rate of 10,000 fps could be achieved. However, the spatial resolution was deteriorated (~1 mm) due to the highly intensification of the optical light emitted from the scintillator. The current work focuses on the improvement of the spatial resolution in high-speed neutron imaging. So, a neutron image intensifier was applied instead of the optical image intensifier and neutron scintillator, as shown in Fig. 1. As a result, the spatial resolution was improved although the frame rate decreases to few hundred fps. This system is suitable for relatively slow phenomena. In the high-speed neutron imaging, the imaging system which is appropriate to research target should be selected and used.

VISUALIZATION OF PARTICLE BEHAVIOR IN MOLTEN GLASS: Neutron imaging experiments were conducted at the B-4 port of the Kyoto University Research Reactor. Soda-lime glass beads were filled in a zirconia melting pot and heated by an electric heating furnace. Figure 2 shows the neutron transmission images of glass melting process and the temperature change in the furnace. At the beginning of the heating, the temperature is lower than the melting point and the apparent volume was large due to the existing void among the glass beads. When the temperature increases around 1,000 ° C, the glass starts to melt and the apparent volume of the glass decreases gradually. Finally, the glass melts completely. As shown in Fig.2, the visualization of molten glass in the furnace can be performed above 1,000 ° C by using the neutron imaging. Then, a tungsten sphere with 10 mm in diameter was dropped into the molten glass in the melting pot. Figure 3 shows the neutron transmission images of the falling sphere in the molten glass. The sphere was clearly observed by neutron transmission imaging. The molten glass has very high viscosity, therefore, the particle motion in the glass is relatively slow. From these images, the velocity could be estimated. The relation between the fluid temperature and the viscosity was evaluated for high temperature molten glass. However, the obtained images have still some noises. The post image processing method would be important for more accurate analysis like a particle size estimation.

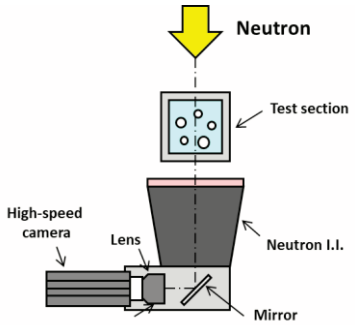

Fig. 1 Neutron imaging system with neutron image intensifier.

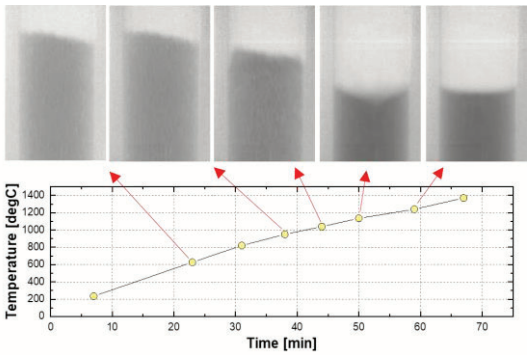

Fig. 2 Melting process of soda-lime glass.

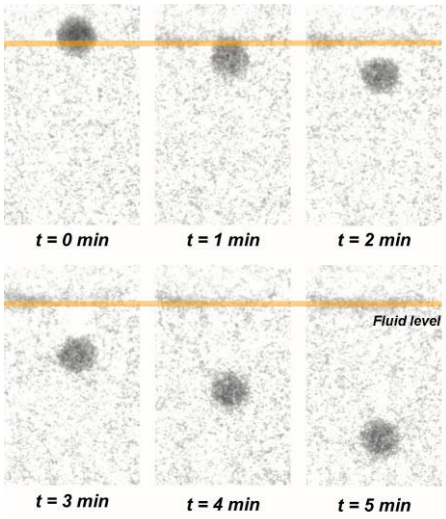

Fig. 3 Neutron transmission images of falling sphere in molten glass at 1200 ° C.

REFERENCES:

[1] Y. Saito, *et al*., Nucl. Instr. Meth. Phys. Res., A, **651** (2011) 36-41

PR8-2 Void Fraction Measurement of Refrigerant Two-Phase Flows in Cross-Flow Parallel Mini-Channel Evaporator

H. Asano, H. Murakawa, S. Inoue, K. Sugimoto, D. Ito[1], Y. Saito[1]

Department of Mechanical Engineering, Kobe University
[1] Institute for Integrated Radiation and Nuclear Science, Kyoto University

INTRODUCTION: Mini-channel compact heat exchangers are attracting attention because of the compactness and reduction in temperature difference between fluids leading to the improvement of the efficiency. Since smaller diameter leads to not only larger heat transfer area density but also larger pressure loss, micro channel heat exchanger has many parallel channels. In the case that the heat exchanger is used for an evaporator, refrigerant flow distribution often causes a deterioration in the heat transfer performance. Especially, when the refrigerant flow is heated by a heating medium flowing in channels with cross-flow arrangement as shown in Fig. 1, non-uniform heat flux might cause the maldistribution of refrigerant flows. In this study, boiling flow behaviors in a single layer microchannel heat exchanger made of stainless steel had been visualized by neutron radiography at B4 port. Void fraction distributions had been measured from the radiographs.

EXPERIMENTS: The tested heat exchanger was manufactured by diffusion bonding of thin stainless-steel plates, and consists of single-layer refrigerant and heating medium parallel channels. The channel cross-section and flow arrangement are shown in Fig. 1 and 2, respectively. HFC-134a and FC3283 were used as the refrigerant and the heating medium, respectively. Each channel has semi- circular cross-section. The heat exchanger was placed in a vertical plane to form vertically upward boiling flows of the refrigerant. The details of the channel patterns are shown in KURNS Progress Report 2019. Radiographs were recorded by a cooled CCD camera with the exposure time of 30 seconds and the pixel size of 88 μm/pixel.

RESULTS: Void fraction was measured for each pixel of visualized images. In gas-liquid two-phase flows in a small diameter non-circular channel, liquid would be accumulated in corners by surface tension. So, volumetric cross-sectional average void fractions were calculated. The distributions for the test sections with the straight, perforated-rib, and offset-rib channels are shown in Fig. 3 (a) to (c), respectively. The horizontal distribution of the void fraction for each test section are also shown in Fig. 4. It can be clearly observed that the void fraction on the right side close to the heating medium inlet was higher than the left side due to the larger temperature difference. The inhomogeneous distribution could be improved by perforation to the ribs. The offset rib was not effective.

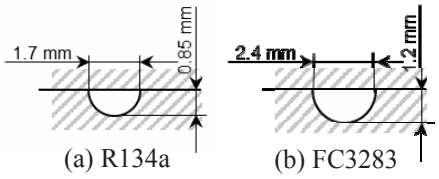

(a) R134a (b) FC3283

Fig.1 Channel cross-section

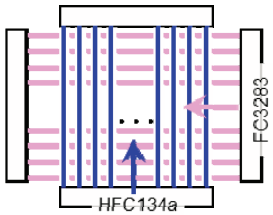

Fig. 2 Channel arrangement

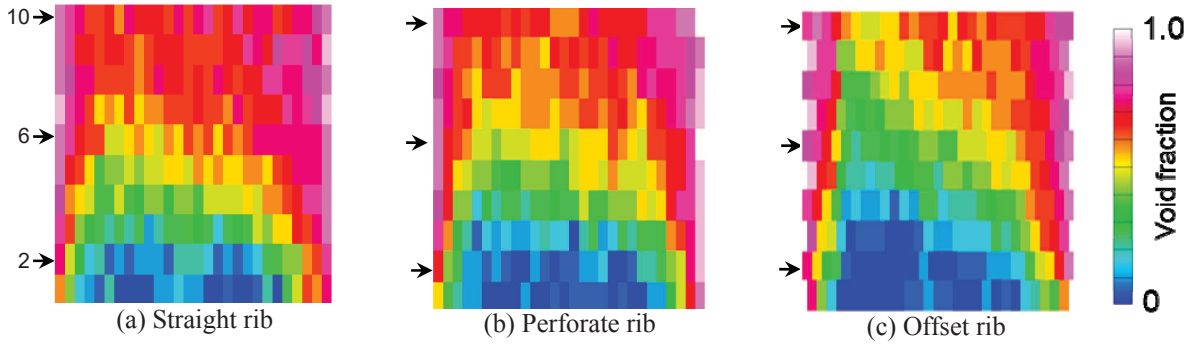

(a) Straight rib (b) Perforate rib (c) Offset rib

Fig. 3 Volumetric average void fraction distribution.

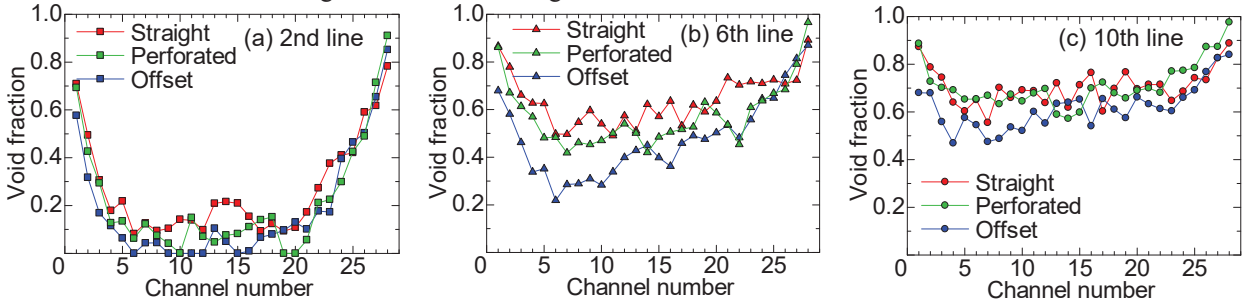

Fig. 4 Effect of the channel pattern on horizontal void fraction distribution.

PR8-3 Visualization of Transient Change of Refrigerant Distribution in Activated Carbon Particle Layer

H. Asano, H. Murakawa, K. Sugimoto, D. Ito[1], Y. Saito[1]

Department of Mechanical Engineering, Kobe University
[1] Institute for Integrated Radiation and Nuclear Science, Kyoto University

INTRODUCTION: Adsorption refrigerator is one of the efficient tools for waste heat recovery because the refrigerator can be driven by heat at relatively low temperature. Refrigerant vapor from an evaporator at low pressure is adsorbed in an adsorbent particle layer in an adsorber. In order to keep vapor adsorption rate and evaporation pressure, a batch process is applied using two or more adsorbers. The adsorbers alternate between the drying process by heating and the adsorption process with cooling. Adsorption amount of refrigerant increases with decreasing the adsorbent temperature for a setting refrigerant pressure. However, in the adsorption process, the adsorbent is heated by adsorption heat which is equivalent to the enthalpy difference between vapor and liquid of refrigerant. So, quick removal of the adsorption heat from the adsorbent is required to enhance the adsorption. Metallic fins are often used for higher heat diffusion. Since the installed metallic fins lead to the increase in heat capacity of the adsorber, fin placement should be optimized. Although it is required to understand the distribution of adsorption amount in adsorption process, it is difficult to measure it, and only the change of total amount has been measured. In this study, the distribution of adsorption amount in an adsorbent particle layer in a cylindrical cell was visualized by neutron radiography at the E2 port.

EXPERIMENTS: Activated carbon and ethanol were used as the combination of adsorbent and refrigerant. The mean particle diameter and specific surface area of the activated carbon were 86 μm and 3170 m^2/g, respectively. Activated carbon was installed in a cylindrical cell with thin stainless-steel wall and the inner diameter of 21 mm. The depth of the adsorbent layer was about 20 mm. The installed amount of dry activated carbon was 1.8 g. The bottom of the cell was brazed on a brass plate whose temperature was maintained by cooling water. The cell was connected to a liquid ethanol reservoir immersed in a temperature-controlled water. The configuration of the cell is shown in Fig. 1. An aluminum pin with the diameter of 3 mm and the height of 20 mm was placed at the center of the cell.
The mass attenuation coefficient of liquid ethanol was 3.86 cm^2/g [1]. Radiographs on a scintillation converter were recorded by a cooled CCD camera with the exposure time of 10 seconds and the pixel size of 42.8 μm/pixel. The surface temperatures of the bottom plate and ethanol reservoir were maintained at 19.5°C and 20°C during the adsorption process, respectively.

RESULTS: Transient change in original radiographs from the dry condition in adsorption process are shown in Fig. 2 (a) to (g). The image becomes darker by increasing the adsorption amount. It can be seen that the adsorption was progressing from the surface of the adsorbent layer. The effect of the aluminum pin was little. Although it was expected that the adsorption amount would be larger near the heat transfer surface, i.e., near the bottom of the adsorbent layer because of the lower temperature, the adsorption amount was higher near the surface of the adsorbent layer. Two reasons are cited. The first is the change in porosity. The height of the layer was seemed to become lower by the adsorption. Increase in vapor flow resistance due to the decrease in porosity might disturb the supply of vapor into the layer. The second is an existence of inert gas. If the inert gas was involved, the concentration might become higher in the layer. The inert gas might disturb the adsorption. The temperature profile is required to consider the phenomena.

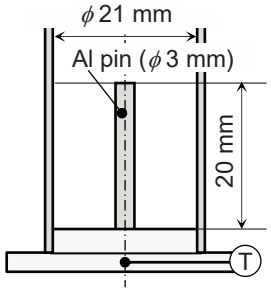

Fig. 1 Test cell

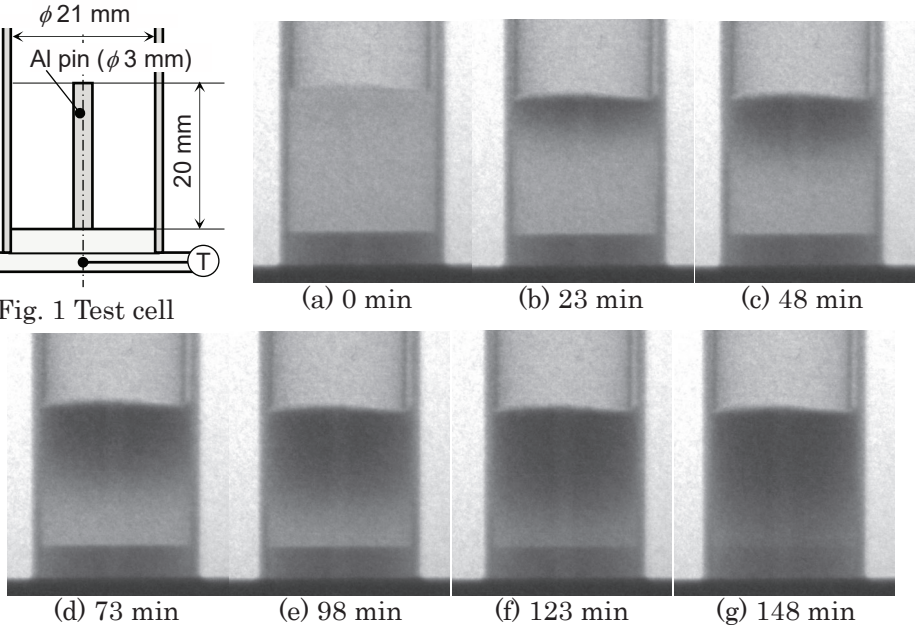
(a) 0 min (b) 23 min (c) 48 min
(d) 73 min (e) 98 min (f) 123 min (g) 148 min
Fig. 2 Transient change in adsorption process.

REFERENCE:
[1] H. Asano, K. Murata, N. Takenaka and Y. Saito, " Visualization and measurement of adsorption/ desorption process of ethanol in activated carbon adsorber", Physics Procedia, **69** (2015) 503-508.

PR8-4 Neutron radiography measurements of the mixing behavior of reactant streams during hydrothermal synthesis

S. Takami, K. Sato, M. Kubo[1], T. Tsukada[1],
K. Sugimoto[2], N. Odaira[3], D. Ito[3], Y. Saito[3]

Graduate School of Engineering, Nagoya University
[1] Graduate School of Engineering, Tohoku University
[2] Graduate School of Engineering, Kobe University
[3] Institute for Integrated Radiation and Nuclear Science, Kyoto University

INTRODUCTION: We have performed the neutron radiography measurements of the mixing behavior of cold and supercritical water in a tubular flow reactor to elucidate the effects of mixing on the supercritical hydrothermal synthesis [1-4]. In the previous measurements, the density and temperature of water at the mixing point were visualized, which suggested the mixing behavior of the two streams. However, the temperature of the streams can be also affected by the heat conduction through the tube wall. Therefore, the experiments that directly show the mass transport should be performed. Here, in this experiment, we performed the neutron radiography measurements of the mixing behavior of the aqueous solution of $Gd(CH_3COO)_3$ with heated water and observed the distribution of Gd^{3+} ions at the mixing point.

EXPERIMENTS: Fig. 1 shows the schematics of the experimental apparatus. A stream of water was fed using a high-pressure pump and heated by an external heater. Simultaneously, the aqueous solution of $Gd(CH_3COO)_3$ (0.025~0.2 M) was fed using another high-pressure pump. The two streams were mixed at the mixing point to initiate the hydrothermal reaction. The inner diameter of the tubes at the mixing point was 2.3 mm. Toward this mixing point, a neutron beam was irradiated and radiography images were obtained using ^{6}LiF/ZnS scintillator screen.

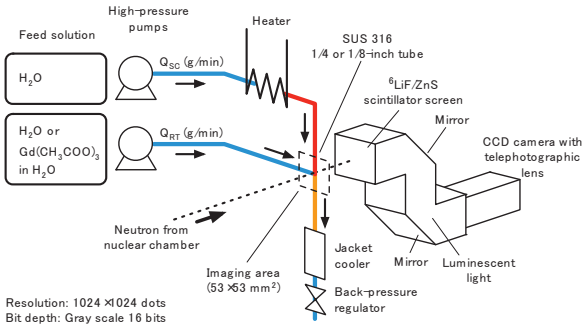

Fig. 1 Schematics of the experimental apparatus.

RESULTS: First of all, we mixed the aqueous solution of $Gd(CH_3COO)_3$ with the stream of water at room temperature. Figure 2a shows the radiography image of the solution that contained Gd^{3+} ions. As we noticed, the darker area existed in the side and the lower tubes. These areas corresponded to the streams that contained Gd^{3+} ions. By subtracting the absorption profile by water, the distribution of Gd^{3+} ions was obtained (Fig. 2b). This image confirmed that the reactant solution was fed from the side tube and went downward on the right-side wall in the lower tube after mixing. This image also showed that the Gd^{3+} ion can be used as the tracer ion to study the mixing behavior in the tubular flow reactor.

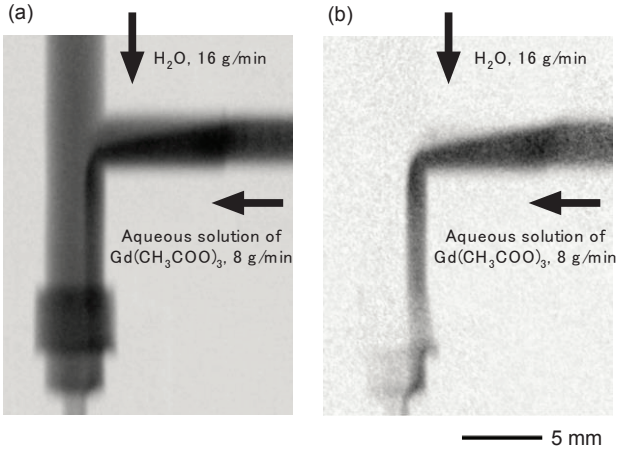

Figure 2 Neutron radiography images of the mixing point showing the absorption by (a) solution and (b) Gd^{3+} ions.

We then performed similar mixing experiments at higher temperatures. Figure 3 shows a snapshot of the neutron radiography measurement during the hydrothermal synthesis of $Gd(OH)_3$ from $Gd(CH_3COO)_3$ aqueous solution. The heated water with smaller density penetrated the upper part of the side tube. The Gd^{3+} solution went through the lower part and mixed with the heated water. The absorption by Gd^{3+} directly indicated the flow of reactant solution. However, as we continued the experiments, the blocking by produced $Gd(OH)_3$ occurred and we could not obtain the neutron radiography images at the steady-state conditions.

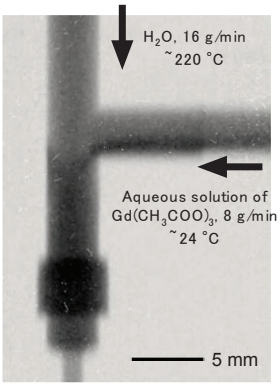

Figure 3 The neutron radiography image of the mixing point during hydrothermal synthesis.

CONCLUSION: By using the aqueous solution of Ga^{3+} ions, the mixing behavior of the reactant solution was directly visualized using neutron radiography. However, the measurement at the steady-state conditions was not successful this time due to plugging.

REFERENCES:

[1] S. Takami *et al.*, J. Supercrit. Fluids, **63** (2012) 46-51.
[2] K. Sugioka *et al.*, AIChE J., **60** (2014) 1168-1175.
[3] S. Takami *et al.,* Phys. Proc., **69** (2015) 564-569.
[4] K. Sugioka *et al.*, J. Supercrit. Fluids, **109** (2016) 43-50.

PR8-5 Quantatively Visualization of a Microchannel Heat Exchanger under Non-uniformly Heated Condition

H. Umekawa[1], T. Ami[1], H. Sakai[1], R. Funakura, Y. Saito[2] and D. Ito[2]

[1]*Department of Mechanical Engineering, Kansai University*
[2]*Institute for Integrated radiation and Nuclear Science, Kyoto University*

INTRODUCTION: Microchannel heat exchanger has several advantages against the conventional fin-tube heat exchanger, thus recently it has been used as the heat exchanger of air-conditioning unit. But this microchannel heat exchanger is consisted from a lot of parallel microchannels, thus it would easily cause the flow oscillation, such as pressure drop oscillation and density wave oscillation. Moreover, the heat transfer coefficient of air at the front edge of heat exchanger plate takes larger value than that of the tail edge owing to the development of thermal boundary layer. and it cause the nonuniform heat flux condition.

In this series of investigation, the effect of heat flux distribution on the heat transfer and flow characteristics have been estimated by using single plate micro channel heat exchanger.

In this report estimation results of a void fraction of microchannel heat exchanger under non-uniform heating by using neutron radiography are briefly introduced.

EXPERIMENTS: Experiments of the visualization were carried out using the B-4 beam line in KUR (1 MW). The schematic diagram of experimental apparatus is shown in Fig.1. The working fluid used in this study was Methanol (99.5% purity), which has low viscosity similar with actual refrigerant (R32) and enough attenuation coefficient for visualization. The experimental apparatus is consisted of a reserve tank, a pump and a test section. Test section is an actual aluminum microchannel heat exchanger of the air-conditioning unit, and it was heated by Joule heating by using two nichrome foils attached to the plate surface with electrical insulation of Kapton film. These nichrome foil heaters could be heated independently, and which achieved the non-uniform heating condition.

RESULTS: Fig. 2 shows the void fraction profile under certain heating condition. All results was obtained with same exit thermal equilibrium quality (x_{exave}=0.188), but (a) was heated by uniform heat flux, and the heat flux ratio (q_L:q_H) of (b) is 1:2 and ratio of (c) is 1:4, respectively. Histograms of void fraction at the high heat flux side of Fig.2 are drawn in Fig 3. As shown in these Figures, influences of the heat flux distribution on the void fraction profile is clearly obtained quantitatively. In this stage, the void fraction profile is obtained as time average image, but quantitatively data of the flow oscillation will be obtained by using dynamic image in next step.

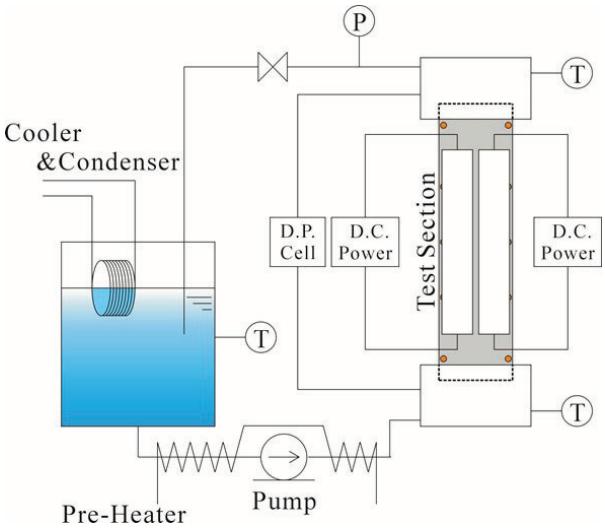

Fig.1 Schematic diagram of experimental apparatus.

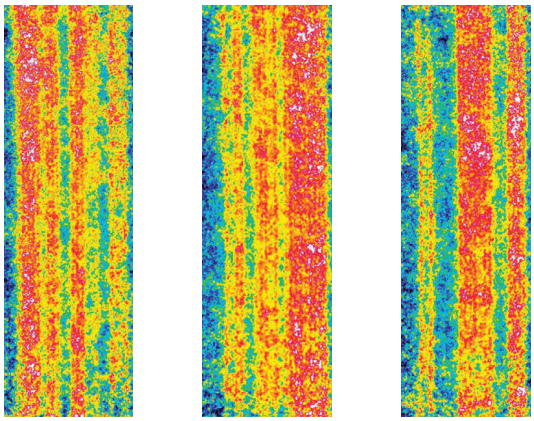

a.Uniform b. 1∶2 c. 1∶4

Fig.2 Example of the visualization results of void fraction xeqave=0.188

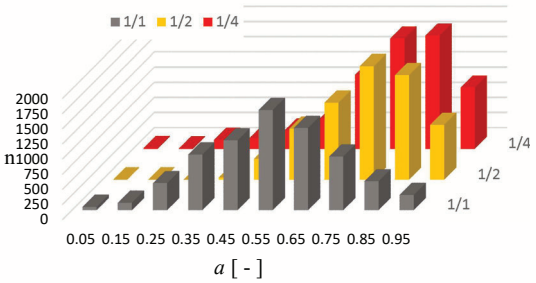

Fig.3 Histogram of void fraction at high heat flux side in Fig.2.

PR8-6 Frost Deposition Distribution Estimated by X-ray and Neutron Cooperative Imaging

R. Matsumoto[1], R. Kuroda[2], T. Makihara[2], H. Ikishima[1], T. Shirai[1], D. Ito[3], N. Odaira[3] and Y. Saito[3]

[1]*Faculty of Engineering Science, Kansai University*
[2]*Graduate School of Science and Engineering, Kansai University*
[3]*Institute for Integrated Radiation and Nuclear Science, Kyoto University*

INTRODUCTION: Recently, heat pumps have been proposed as an effective air conditioning system of heating operation for electric vehicles (EV), because of the inability to use the engine heat as in the conventional vehicles. However, during the heating operation, frosting occurs on the outdoor heat exchanger of the air conditioning system. The frost formation causes a serious energy loss on the battery of EV due to the heat transfer performance degradation by increasing the thermal resistance. In addition, the corrugated fin heat exchanger which is mainly used as an automotive heat exchanger, has a more complicated structure than conventional one, so it is difficult to capture the frosting situation. In this study, the three dimensional distribution of the frost deposition on the corrugated fin heat exchanger were estimated by X-ray and neutron cooperative imaging.

EXPERIMENTAL PROCUDURE: Fig.1 shows the schematic view of the experimental setup. The frost deposition between the fins is measured by irradiating X-ray parallel to the fins of the heat exchanger. The heat exchanger is made of aluminum. Thus, the frost deposition inside of the heat exchanger can be measured by irradiating neutron beam perpendicularly to the fins though the heat exchanger. Cooled humid air adjusted to the flow velocity 1 m/sec is supplied to the test section. The test section consists of the styrofoam block duct and the corrugated fin heat exchanger. The heat exchanger was cooled by circulating the -27 ºC fluorinert. The frost deposition on the heat exchanger was observed by CCD camera (Princeton Inst., 16-bit, 1024×1024 pixels and 512×512 pixels) with image intensifier (Toshiba Electron Tubes & Dev., E5877CS-P1K and E5830NE-P4K) in every 1 min for 20 min frosting duration. Exposure time is 0.5sec for X-ray and 1.7sec for neutron beam.

RESULTS: Fig.2 shows the front view of the corrugated fin heat exchanger. The corrugated fin heat exchanger consists of flat tubes and the brazed corrugated louver fins. The coolant flows in the parallel flat tubes and the humid air flows in the small fin channels formed by the corrugated louver fins. Fig.3 shows the frost deposition distributions on the heat exchanger. X-ray images show the frost formation observed from the front view of the heat exchanger. On the X-ray images, frost was formed uniformly on the fins. The neutron images show the frost deposition inside of the heat exchanger. The main flow direction is left to right on the neutron images in Fig.3. At 100 sec, the frost formed in the upstream side of the fin channels. At 1200 sec, the frost deposits on the fin front, which induces the heat transfer problems by the air side pressure loss. This results shows the frost deposition distribution in the corrugated fin heat exchanger clearly by X-ray and neutron cooperative imaging.

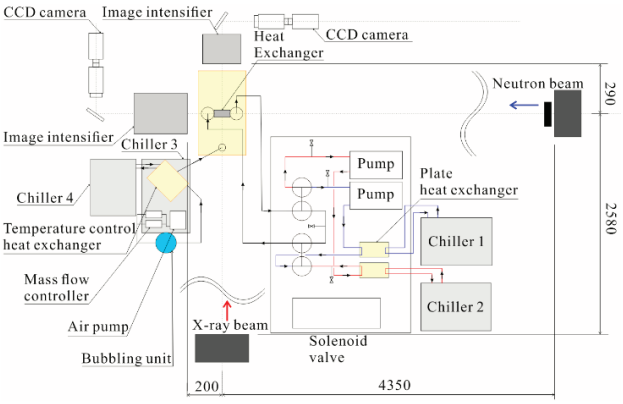

Fig.1 Schematic view of the experimental setup

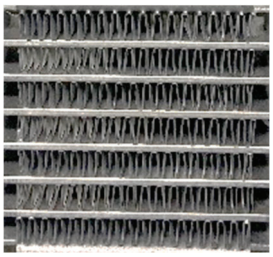

Fig.2 Front view of the corrugated fin heat exchanger

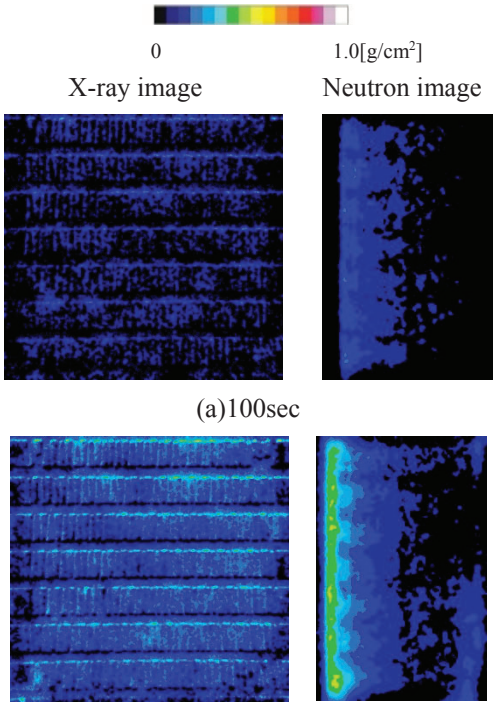

(a)100sec

(b)1200sec

Fig.3 Forst deposition distributions observed by X-ray and neutron radiography.

PR8-7 Analysis of vapor pressure in fire spalling of high-strength concrete

Y. Nishio[1], M. Kanematsu[1], A. Miyabe[1], K. Kobayashi[1], A. Yang[1], H. Fumino[1], N.Odaira[2], D. Ito[2], Y. Saito[2]

[1] Department of Architecture, Tokyo University of Science
[2] The Institute for Integrated radiation and nuclear science joint-use research, Kyoto University

INTRODUCTION: Fire spalling with High-strength concrete was a well-known phenomenon, and thermal stress and water vapor pressure in concrete have considered to be the main causes of spalling. To capture detailed moisture movement in concrete under fire is important to clarify the mechanism of spalling [1]. In this study, we investigated the relationship between spalling phenomena and moisture transfer under heating by using neutron radiography. Measuring moisture transfer inside concrete quantitatively, how vapor pressure inside concrete affect spalling was considered.

EXPERIMENTS: Concrete specimens (70×100×30 mm^3) with W / B of 18% were prepared. In some of them, a single rebar (D10, 120mm) with a thermocouple was embedded at 20mm from the heating surface. Adjusting water content before heating, specimens with three different water content (named as "dry", "air" and "sat" respectively) were prepared. The initial relative humidity (RH) of those were 25%, 75% and 100% respectively. In this experiment, the specimens were heated at the bottom surface with quartz heater. Neutron radiography was performed at the B-4 port of KUR. Setup for the experiment is shown in Fig.1. Apart from NR measurement, temperatures in specimen were measured by thermocouples installed in holes with 1.2 mm diameter at the position of 10, 20, 30 and 50 mm from the heating surface.

RESULTS: Using relationships between values measured by neutron radiography and paste volume ratio to concrete (Vp) with different RH (0, 25, 80 and 100%) shown in Fig. 2 and Fig. 3, water amount in concrete specimen during heating was calculated quantitatively. Fig. 4 shows calculated RH inside concrete at each water content for each distance from heating surface just before spalling. Temperatures at 2 and 5 mm from the surface in Fig. 4 were analytical values calculated by measured values. Fig. 5 shows vapor pressure distribution just before spalling calculated by the result of Fig. 4. From the figure, the vapor pressure in "air" is higher than that in "sat" or "dry", and the observed maximum value is about 1.8Mpa. This is about the same value reported in the past researches.

REFERENCES:

[1] JCI, (2017). "Committee Reports:JCI-TC-154A"

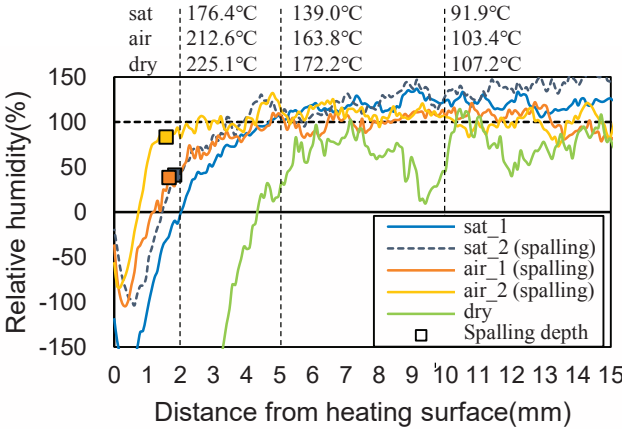

Fig. 4. Moisture content distribution from heating surface immediately before spalling.

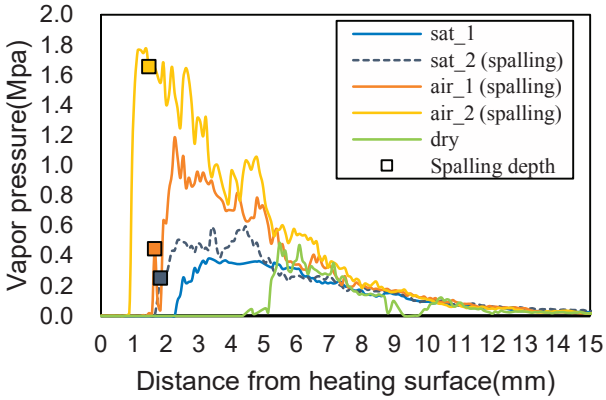

Fig. 5. Vapor pressure distribution from heating surface immediately before spalling.

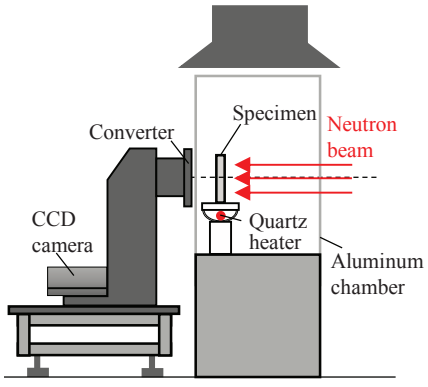

Fig. 1. Outline of Experimental setup.

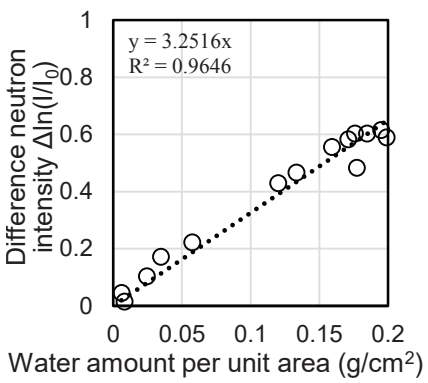

Fig. 2. Relationship between differential intensity and water amount.

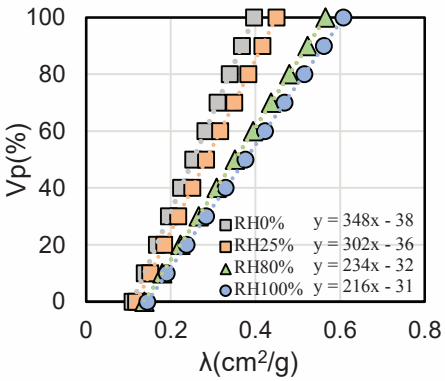

Fig. 3. Relationship between paste volume and absorption coefficient.

PR8-8 Measurement of coolant inside a flat laminate vapor chamber in the vertical posture with Neutron Radiography

K. Mizuta, Y. Saito [1], D. Ito [1]

Faculty of Engineering, Kagoshima University
[1]Institute for Integrated Radiation and Nuclear Science, Kyoto University

INTRODUCTION: Recently, cooling of electronic devices has been crucial than ever because size of such devices is rapidly shrinking though the power input to the devices is almost the same or even getting larger, which leads to the rapid increase in power density. This trend makes it difficult to achieve adequate heat exhausting ability especially at the heat receiving region of such heat exhausting system. Thus, various types of vapor chambers are getting more attention than ever with a hope for solving such problems by their higher heat spreading ability than conventional methods such as copper heat spreader. In the practical use of vapor chambers, postural influence on thermal performance of vapor chambers is very important, because the change in the thermal performance of vapor chamber with posture, if it occurs, may restrict the performance of the electronic devices not to exceed its limit of junction temperature. A flat laminate vapor chamber called FGHP (Fine Grid Heat Pipe) is one of the most promising candidates to solve such thermal problems, with the highest heat spreading ability concerning the overall heat transfer coefficient based on heat source area [1]. Our previous study shows that the effect of gravity on the coolant distribution of FGHP is negligible [2].

In this study, we investigated the gravitational effects on the coolant distribution in the FGHP by using neutron radiography at the Kyoto University Research Reactor (KUR) for various types of FGHP.

EXPERIMENTS: Experiment was conducted at the E-2 port of the KUR, where the thermal neutron flux at the sample position was about 3×10^5 cm^2s at 5 MW operation. Test samples of FGHP were disc shaped, diameters were 40, 80 mm, respectively and the thickness of ether samples were 2 mm. Inner structure of both sample was almost the same as the test samples utilized in our previous study[2]. The test samples were set vertically, which means that its bottom and top plate was placed parallel to the gravitational direction. Figure 1 shows the experimental setup. A CCD camera (BU-53LN, BITRAN Co. Ltd.) was utilized, which has 4008×2672 pixels and ^{6}LiFZnS (50 μm thickness) was used as a scintillator screen. The spatial resolution was 9.0 μm/pixel at the present system setup, however, the effective spatial resolution was about 50 μm/pixel due to the scintillator screen characteristics. Neutron imaging of the sample was performed at the 1 MW operation mode of the KUR and the exposure time was 300 s. Neutron images of the sample were utilized to calculate liquid thickness in the FGHP. The effect of gravity on the coolant distribution was evaluated by the calculated liquid thickness in the wick area at different four positions. The liquid thickness was evaluated by the same scheme as in our previous study[2].

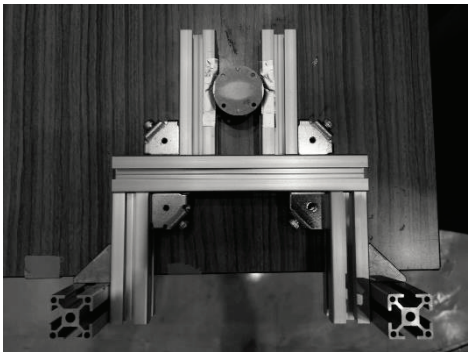

(a) ϕ = 40 mm

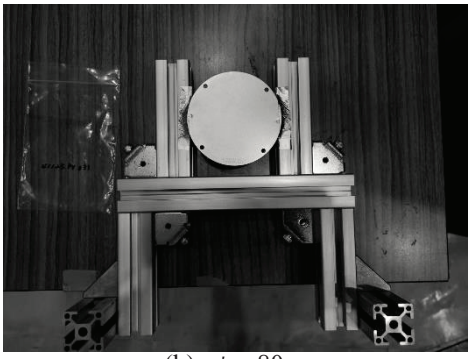

(b) ϕ = 80 mm

Fig. 1 FGHP test samples.

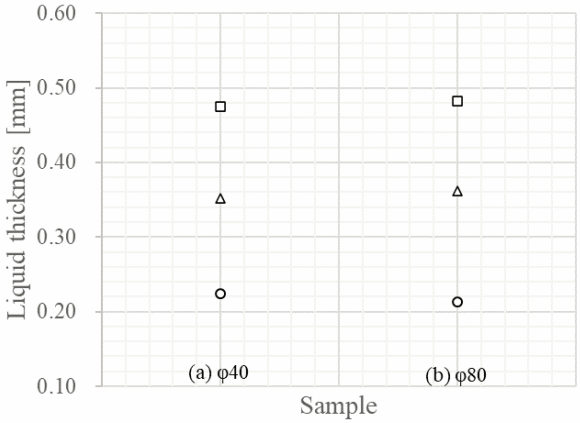

Fig. 2 Liquid thickness for both samples.
(○:top, □:bottom, △:horizontal average)

RESULTS: Evaluated liquid thickness of both samples were shown in Fig. 2. Figure 2 shows that liquid thickness at various positions were almost same regardless of the diameter of FGHP test sample, and the liquid thickness was also almost the same as those in our previous work of 65 mm square sample [2]. This fact means that the liquid thickness depends mainly on the inner structure of FGHP rather than its outer size and shape.

REFERENCES:

[1] Mizuta, K., et al., Applied thermal management, **104** (2016) 461-471.
[2] Mizuta, K., el al., Physics Procedia, **69** (2015) 556-563

R2P8-9

PR8-9 Quantitative Study of the Image Quality for Neutron Imaging

M. Kitaguchi, K. Hirota[1], H. M. Shimizu[1], D Ito[2], and Y. Saitoh[2]

KMI, *Nagoya University*

[1]*Graduate School of Science, Nagoya University*
[2]*Institute for Integrated Radiation and Nuclear Science, Kyoto University*

INTRODUCTION: Mechanical and industrial products such as automobiles and aircraft are progressing with higher performance and higher accuracy in Japan. One of the demands at the development site of these state-of-the-art products is a visualization of the state of organic materials (oil film, grease, electrolyte, etc.) existing between metals, which can not be seen directly by our eyes. Neutron imaging is one of the solutions to observe the dynamic state of the organic materials (shape, properties, thickness distribution) and its dynamic change. We have started to obtain of the imaging of automobile parts as an example in KUR E2 port. We are also proceeding with the quantitative evaluation of the CCD output image.

In order to expand the evaluation technique to wide range of applications, the quality of image should be studied systematically. The quality should be estimated by using the information of neutron flux, the upstream optics, the performance of detector system, and their arrangement. In the case of visible light optics, the performance of optical system is qualified by using the 'modulation transfer function (MTF)' (Figure 1). The MTF for visible light optics can be calculated precisely by simulations. On the other hand, the systematic qualification for neutron imaging has not been standardized. Because of the large volume of the source, the divergence of the rays, and the finite resolution of the detector system, the performance of the whole system of neutron imaging can not be written as a simple combination of MTF for each subsystem. The general formula to qualify the whole system should be established even for the case of low-intensity compact neutron source.

EXPERIMENTS AND RESULTS: For the demonstration, the transmission images of a standard indicator were taken with various conditions of the distance between the sample and the detector. Figure 2 shows the change of the contrast according to the distance. We can also find that the contrast depends on the measurement time because of the statistical uncertainty with low flux of neutrons.

The E2 port as an optical source is not a pinhole but a spread area. This means that the MTF of each component, for example, source, beamline, and detector, can not be extracted simply. We are going to combine more measurements under various conditions to understand the quality of image quantitatively.

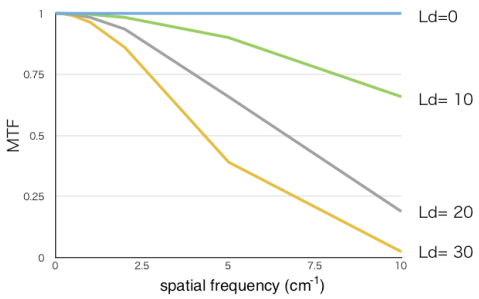

Figure 1: Typical shape of MTF according to the distance between sample and detector for a simple pinhole system.

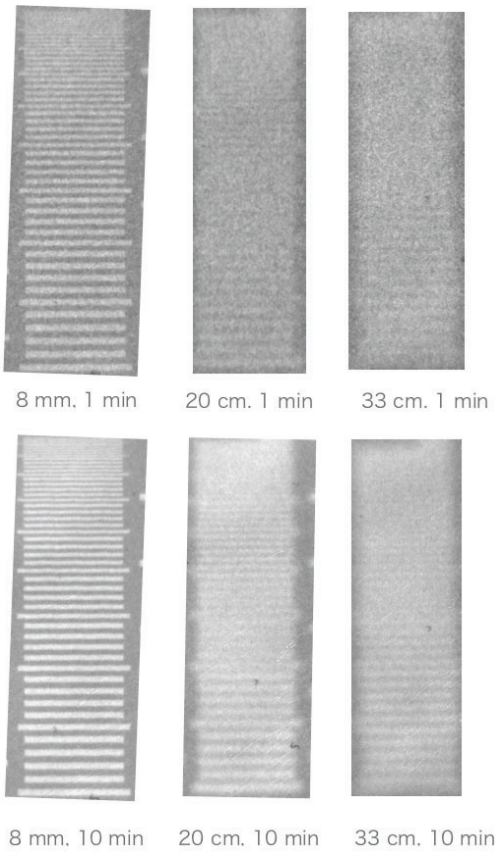

Figure 2: The transmission image of a standard indicator with various conditions. Not only the distance between sample and detector but also the measurement time affect the quality of image.

PR8-10 Dynamic Visualization of Hydrogen Accumulation Behavior in Metallic Materials via Neutron Imaging

K. Shimizu[1], H. Toda[2], K. Hirayama[2], H. Fujihara[2], D. Ito[3], Y. Saito[3]

[1]*Department of Physical Science and Materials Engineering, Iwate University*
[2]*Department of Mechanical Engineering, Faculty of Engineering, Kyushu university*
[3]*Institute for Integrated Radiation and Nuclear Science, Kyoto University*

INTRODUCTION: It is widely recognized that hydrogen in metallic materials degrades the mechanical properties of the materials. Various hydrogen embrittlement mechanisms, such as HELP, HEDE and HESIV have been proposed to date [1], but there is still no comprehensive interpretation. However, for each mechanism, it is consistent that hydrogen trapping and the resulting localization of hydrogen to defects and microstructures are the dominant factors of hydrogen embrittlement [2]. To understand the hydrogen embrittlement, it is necessary to visualize the hydrogen distribution and to elucidate its evolutionary behavior over time. In this study, hydrogen in a metal was visualized by neutron radiography and tomography, and hydrogen accumulation under stress was assessed. Several palladium specimens with different hydrogen contents were prepared and a notch was introduced. It has been demonstrated that hydrogen content can be analyzed by neutron tomography, and the possibility of evaluating hydrogen accumulation under stress is discussed.

EXPERIMENTS: Palladium specimens with hydrogen contents of 0 at%, 10 at% were prepared for neutron imaging. Hydrogen content was controlled by high temperature hydrogen exposure. Neutron radiography was performed on the KUR B-4 port [3]. The imaging system consists of a ^{6}LiF:ZnS visible light converter and a cooled CCD detector. The exposure time was set to 5 min at a thermal power of 1 MW in the research reactor.

RESULTS: Fig. 1 shows pure Pd and Pd-23%Ag alloys visualized at the B-4 port of KUR. Charged hydrogen concentrations are 0% and 10%. In both alloys, the contrast of neutron transmission images is darkened due to hydrogen charging. The difference in hydrogen concentration of 10% can be clearly visualized by static observation in B-4 port. After static imaging, the Pd specimen with 10% hydrogen concentration shown in Fig. 1(b) was subjected to tensile loading by a test-jig and was observed continuously. Fig. 2 shows the neutron transmission images of unloading, the first loading, and the second loading, indicating that the notch introduced in Pd was opened by monotonic tensile loading. The stress state of notch-tip becomes triaxial and forms a hydrostatic stress field in tension by tensile loading. We expected to see a dark contrast in the neutron transmission image due to the accumulation of hydrogen in this hydrostatic stress field before the present experiment, but this was not observed in Fig. 2. The reason for this is that the absolute value of the hydrostatic stress is low, or the size of the formed hydrostatic stress field is much smaller than the spatial resolution of this imaging. This hydrogen accumulation behavior will be investigated deeply in the future work.

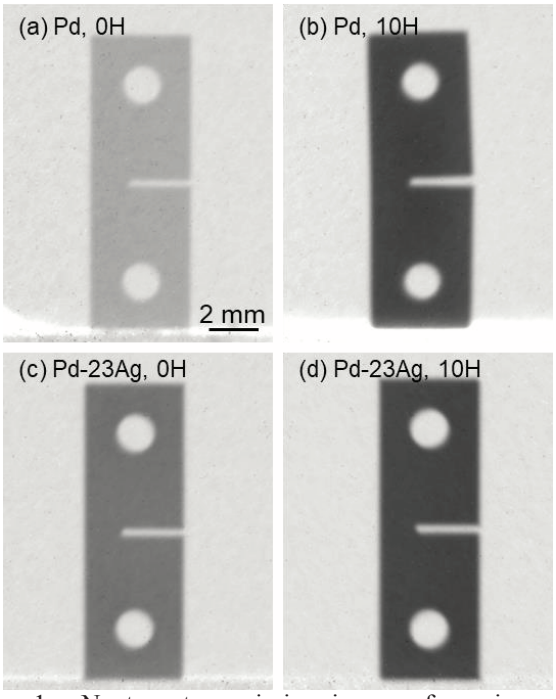

Fig. 1. Neutron transmission image of specimens visualized at B-4 port. (a) and (b) are pure Pd with 0% and 10% hydrogen concentration, respectively. (c) and (d) are Pd-23%Ag alloys with 0% and 10% hydrogen concentration, respectively.

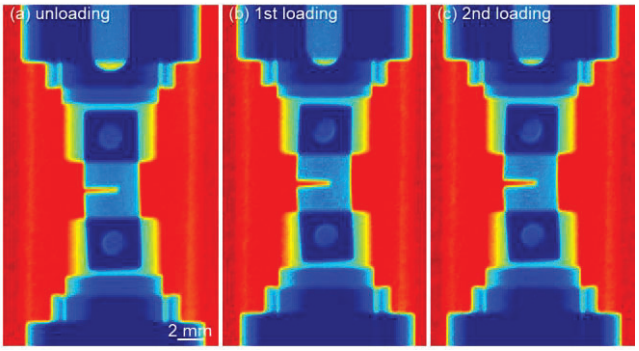

Fig. 2. Neutron transmission image of the specimen captured at (a) unloading, (b) after 1st loading, and (c) after 2nd loading. The contrast of these neutron transmission image is shown in color scale.

REFERENCES:

[1] I. M. Robertson *et al.*, Metall. Mater. Trans. A 46 (2015) 1085-1103.
[2] Z. Zhang *et al.*, Acta. Mater. 113 (2016) 272–283.
[3] Y. Saito *et al.*, J. Jpn. Soc. Precis. Eng. 79 (2013) 822–825.

PR8-11 *In-situ* Lithium diffusion behavior in NASICON-Type Structured Lithium Ion Conductive Composite by Means of Neutron Radiography

S. Takai[1], F. Song[1], H. Chen[1], K. Ota[1], T. Yamamoto[1], T. Yabutsuka[1], T. Yao[2], D. Saito[3], Y. Saito[3]

[1]*Graduate School of Energy Science, Kyoto University*
[2]*Kyoto University*
[3]*Institute for Integrated Radiation and Nuclear Science, Kyoto University*

INTRODUCTION: Heterogenous doping effect, originally observed in halide solid state electrolytes, is proven to be favourable in oxide solid-state electrolytes by Onishi and Song *et. al.* [1,2]. Heterogenous doping is to disperse insulative particles in Li^+ ion conductors and create space charge layers at the vicinity of the insulative particles, which eventually improves the overall ionic conductivity of solid-state electrolyte [3]. Such dispersion system is referred as composite solid-state electrolytes.
In this work, an electrolysis apparatus was built and utilised to electrolyse ^{N}Li LATP / ^{7}Li LATP diffusion couple, where N and 7 is the abbreviation of natural and 7 of isotopes. By applying a galvanostatic current across this diffusion couple at elevated temperature, the ^{6}Li in ^{N}Li LATP can be driven and diffuse towards and through ^{7}Li LATP. The process of ^{6}Li diffusion can be observed *in-situ* by the transmissive neutron beam in KUR (B4 port), owing to the significant difference in absorption cross-section in neutron beam between ^{6}Li and ^{7}Li.

EXPERIMENTS: ^{7}Li and ^{N}Li $Li_{1.3}Al_{0.3}Ti_{1.7}(PO_4)_3$ pellets were synthesised by solid-state reaction method. ^{N}Li Li_2TiO_3 and Mn_2O_3 pellets were also produced by sintering from precursor. The surfaces of LATP were polished to ensure the flatness and mirror finish. During neutron radiography, the LATP, LTO pellets were assembled as the configuration shown in Fig. 2. The assembly was heated to 300 °C while subjected to 0.25 μA of DC current to lead the solid-state electrolysis. After the electrolysis was started, the entire apparatus was subjected to direct neutron beam for 45 minutes at B4 port of KUR (reactor power output was 1MW). Neutron radiography images were taken by the CCD camera (5 min exposure) every 15 minutes.

RESULTS: As shown in Fig. 2, the neutron radiography images from t = 0 to 75 minutes show no change in contrast in the ^{7}Li LATP section, indicating that the electrolysis was insufficient to drive the diffusion of ^{6}Li from ^{N}Li LATP towards ^{7}Li LATP. This is due to the significantly suppressed DC current (0.25 μA) during the electrolysis. Owing to high resistance of LTO pellets, higher DC current can cause an overpotential across the assembly, which might decompose the LTO and subsequently block the current entirely. Furthermore, the large thickness of the pellets is also impeding the current. To improve the issues, materials other than LTO and Mn_2O_3 should be employed to serve as Li^+ reservoir and receiver, such that the assembly can allow higher DC current (around 45 mA to drive sufficient $^{6}Li^+$ migration). And the thickness of the pellets should also be reduced to bring down the over-all resistance of the assembly.

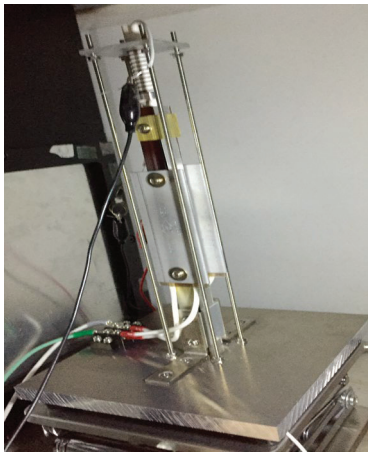

Figure 1 Photo of the apparatus.

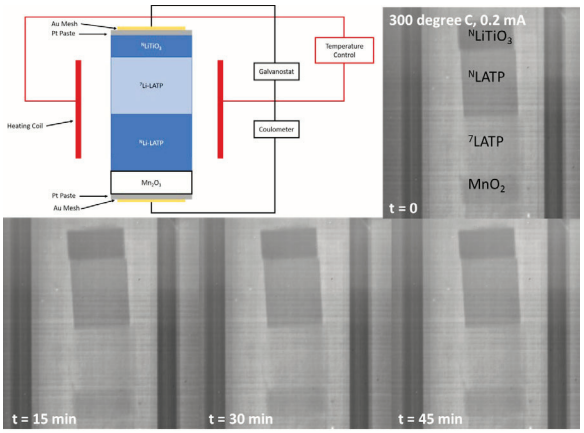

Figure 2 Scheme of the configuration of the solid-state electrolysis set-up and neutron radiography images at *t* = 0, 15, 30 and 45 minutes at 300 °C.

REFERENCES:

[1] H. Onishi *et al*. *Electrochemistry*. 84 (2016) 967.
[2] F. Song *et. al. J. Alloys Compds*. 853(2021)157089.
[3] C. C Liang. *J. Electrochemical Soc*. 120 (1973) 1289.